Scientia Iranica B (2019) 26(6), 3262–3270

SCIENTIA IRANICA

Sharif University of Technology
Scientia Iranica
Transactions B: Mechanical Engineering
http://scientiairanica.sharif.edu

Proposing a new nonlinear hyperviscoelastic constitutive model to describe uniaxial compression behavior and dependence of stress-relaxation response on strain levels for isotropic tissue-equivalent material

Z. Matin Ghahfarokhi[a], M. Moghimi Zand[b,*], and M. Salmani-Tehrani[a]

a. *Department of Mechanical Engineering, Isfahan University of Technology, Isfahan, P.O. Box 8415683111, Iran.*
b. *Small Medical Devices, Bio-MEMS & LoC Lab, School of Mechanical Engineering, College of Engineering, University of Tehran, Tehran, Postal Code 14399-55961, Iran.*

Received 9 January 2018; received in revised form 18 July 2018; accepted 22 August 2018

KEYWORDS
Hyperviscoelastic; Modeling; Tissue-equivalent material; Strain-dependent; Stress-relaxation behavior.

Abstract. Predicting the nonlinear response of biological tissues is a challenging issue due to strain rate- (short-term) and time-dependent (long-term) nature of its response. While many of the tissue properties have already been extensively examined, some are left unnoticed, such as dependence of the stress-relaxation behavior on the strain levels. In this paper, a hyperviscoelastic constitutive model is derived within the integral form presented by Pipkin and Rogers model to remove this limitation. In the suggested model, the hyperelastic and short-term viscous parts are represented by a suitable strain energy function. The long-term viscous function includes the deformation history, which is expressed through a tensorial-relaxation function and has not been considered elsewhere. The constitutive model involves a number of material parameters. The values of those are identified from experimental data for Adiprene-L100 as a tissue-equivalent material. Parameters appearing in constitutive law are estimated by fitting the model with the experimental data. It is assumed that the tissue phantom is slightly compressible, isotropic, and homogenous. The obtained results indicate that the presented model can describe the nonlinearity, strain rate- (short-term) and time-dependent (long-term) effects of materials. The validation of the model is investigated, and very good agreement between the proposed model and the experimental data is shown.

1. Introduction

Over the last two decades, there has been a notable progress in the fields of diagnostic procedures such as planning of computer-assisted surgical treatment, image-guided surgery, and medical robotic technology [1-5]. In all of these cases, the knowledge of mechanical properties of soft tissues is crucial for modeling the nonlinear behavior of tissues. A vast array of investigations has been performed to determine the behavior of biological tissues from a theoretical viewpoint and by experimental investigations. For example, Kemper et al. [6] carried out a total of 36 uniaxial compression experiments on human liver parenchyma within 48 hours of death at four rates ranging from 0.012-10.708 s^{-1}. They showed that the human liver response was both nonlinear, and that

*. *Corresponding author. Tel: +98 021 61114807*
Fax: +98 21 88013029
E-mail address: mahdimoghimi@ut.ac.ir (M. Moghimi Zand)

doi: 10.24200/sci.2018.50235.1592

the dependence on the strain rate and failure strain decreased with the increased loading rate, while failure stress significantly increased. Rashid et al. [7] carried out experimental tests on various loading cases to determine a suitable hyperelastic constitutive model to predict the mechanical properties of porcine brain tissue by using a large sample shear test. The obtained results indicate that the Mooney-Rivlin model has a good capability to predict the linear experimental shear data, as observed at strain rates used in the tests and the Ogden model, which is responsible for both linear and nonlinear experimental shear data. Abbasi et al. [8] used the inverse finite element method and an optimization algorithm to find a suitable hyperelastic model for the characterization of material properties of mouse oocyte cell and mouse embryo cell. In this regard, they used different hyperelastic models such as Ogden, Mooney-Rivlin, Arruda-Boyce, etc. They found that Ogden model and Mooney-Rivlin model were suitable for describing mouse oocyte cell and mouse embryo cell, respectively. In addition, the material properties of the human Medial Collateral Ligament (MCL) were studied by Quapp and Weiss [9]. They performed tensile tests along and transverse to the collagen fiber direction on the obtained specimens of ten human cadaveric MCLs. The experimental data were used to evaluate the ability of three hyperelastic constitutive models. These were referred to as the "one-coefficient and two-coefficient" models proposed by Weiss and the "Lanir" material model to describe the material behavior of human MCL. The results of their investigations indicate that the longitudinal behavior of MCL can well be described by three constitutive models. However, the ability of these models to represent the transverse behavior varies. The performed investigations indicate that a hyperelastic constitutive model can describe the nonlinear behavior of biological tissues. However, the hyperelastic models can describe any time- or rate-dependent and multiphasic behavior. Hereupon, the hyperelastic models have been extended, and viscoelastic models have been presented by researchers to consider such effects. Many studies have been made on these models. Among them, Wang et al. [10] characterized the stress-relaxation behavior of fresh porcine liver and spleen with a Double Maxwell-arm Wiechert (DMW) model. Sharifi Sedeh et al. [11] used a quasi-linear hyper-viscoelastic constitutive model for describing the response of bovine liver tissue at a uniaxial compression test. This theory has also been used for more studies on tissue behavior under simple loading and needle insertion (see [12,13]). The quasi-linear theory is composed of two contributions. Nonlinear behavior of tissues is modeled with a hyperelastic contribution, and a linear time-dependent component is considered to describe the viscoelastic behavior [14-16]. However, the widespread use of quasi-linear viscoelastic theory shows its popularity, and the linear time-dependent feature of this theory limits its applicability for describing strain-dependent stress-relaxation behavior [14].

Further to that, despite a significant amount of research carried out to study the body organs, the preparation of experimental samples and the determination of the material properties of biological tissue is a complex problem due to their nature [17]; therefore, the use of organ-equivalent materials is a usual method. The highly nonlinear and time-dependent behavior of polymeric materials has made it desirable to choose these materials over the biological tissue for using the biomaterial areas [18-20]. For instance, Tirella et al. [21] derived the viscoelastic parameters using the epsilon dot method for soft hydrated biomaterials. To this end, they performed several compression tests on the polydimethlsiloxane and gelatin samples with different strain rates. Then, the obtained dataset was used for analyzing and estimating the viscoelastic parameters. Moreover, they determined the viscoelastic response of porcine liver by this procedure, and showed that hepatic tissue constitutive parameters were quantified without using any pre-stress and before the onset of time-dependent degradation phenomena.

As mentioned above, whereas many of the tissue properties have already been extensively examined, some are left unnoticed, such as the dependence of the stress-relaxation behavior on the strain. Thus, a more general relation is necessary to remove this limitation. The objective of this paper is to develop a new nonlinear hyper-viscoelastic constitutive model that describes the response of compressible, isotropic, and homogenous tissue for the compression and stress-relaxation tests at different strain levels. The model is composed of hyperelastic and viscous parts. The hyperelastic part is represented by the strain energy function, and viscous stress is derived by two strain rate- (short-term) and time-dependent (long-term) parts. More details of performed investigations are discussed in the following sections.

2. Methods and materials

Based on the nonlinearity, strain rate- and time-dependent responses of soft tissue, it is assumed that a nonlinear compressible isotropic hyperviscoelastic constitutive model is suitable for describing the behavior of isotropic and homogeneous tissues [11,22]. The model is derived within the integral form presented by Pipkin and Rogers [23] and developed by Rajagopal and Wineman [24]. Most importantly, the model enables the prediction of the nonlinearity, strain rate-dependence, and the dependence of the stress-relaxation response at strain levels.

2.1. Hyperviscoelastic constitutive model development

In this section, a nonlinear constitutive model is constructed to predict the tissue behavior. The model consists of two hyperelastic and viscous parts. The hyperelastic part is formulated on the basis of a strain energy function decoupled into isochoric and volumetric parts. The viscous part is also represented by two parts capturing the strain rate (short-term) and time-dependent (long-term) behavior. Short-term behavior is described by a strain energy function, which presents the dissipation of energy and long-term behavior based on the strain derived with the integral form. The proposed constitutive model can be generally written at any time, t, as follows [24]:

$$\boldsymbol{\sigma}(t) = -p\mathbf{I} + \mathbf{F}(t) \left\{ \mathbf{R}\left[\mathbf{C}(t), 0\right] + \int_0^t \frac{\partial \mathbf{R}\left[\mathbf{C}(\tau), t-\tau\right]}{\partial(t-\tau)} \mathrm{d}\tau \right\} \mathbf{F}^{\mathrm{T}}(t), \tag{1}$$

where $\boldsymbol{\sigma}(t)$ and $\mathbf{R}[\mathbf{C}(\tau), t-\tau]$ are the Cauchy stress tensor and a tensorial-relaxation function, respectively.

Since biological tissues behave differently in bulk and shear loading, it is beneficial to split the deformation gradient tensor into volumetric and isochoric parts [25]. Thus, Eq. (1) can be rewritten as follows:

$$\boldsymbol{\sigma}(t) = \mathbf{F}(t) \left\{ \mathbf{R}\left[\bar{\mathbf{C}}(t), 0\right] + \int_0^t \frac{\partial \mathbf{R}\left[\bar{\mathbf{C}}(\tau), t-\tau\right]}{\partial(t-\tau)} \mathrm{d}\tau \right\} \mathbf{F}^{\mathrm{T}}(t), \tag{2}$$

where $\overline{\mathbf{C}} = \overline{\mathbf{F}}^{\mathrm{T}}\overline{\mathbf{F}}$ is the modified right Cauchy-Green deformation tensor, while $\overline{\mathbf{F}} = J^{(-1/3)}\mathbf{F}$ is the corresponding modified deformation gradient tensor [26]. $\mathbf{R}\left[\bar{\mathbf{C}}(\tau), t-\tau\right]$ is suggested through:

$$\mathbf{R}\left[\bar{\mathbf{C}}(\tau), t-\tau\right] = \mathbf{S}\left[\left(1-\alpha(\lambda)\right) \mathrm{e}^{-(t-\tau)\beta\left(\lambda,\dot{\lambda}\right)} + \alpha(\lambda)\right], \tag{3}$$

where $\alpha(\lambda)$ and $\beta(\lambda, \dot{\lambda})$ are the functions of the stretch and stretch rate. In addition, second Piola-Kirchhoff stress tensor, $\mathbf{S}$, is calculated from the strain energy function (ψ) expressed as follows [26,27]:

$$\psi = \psi_{\mathrm{vol}}(J) + \psi_{\mathrm{iso}}\left(\bar{\mathbf{C}}\right) + \psi_{\mathrm{visco}}\left(\dot{\bar{\mathbf{C}}}\right). \tag{4}$$

In Eq. (2), it is assumed that no deformation occurs prior to time $t = 0$, and $\mathbf{F}(t)\mathbf{R}\left[\bar{\mathbf{C}}(\tau), 0\right]\mathbf{F}^{\mathrm{T}}(t)$ can be considered as the instantaneous stress at time t. Moreover, it is noted that the reference configuration is a stress-free configuration, and $\mathbf{R}\left[\bar{\mathbf{C}}(\tau), 0\right]$ is zero in the absence of deformation.

In Eq. (3), $\mathbf{S}$ can be transformed into hyperelastic and viscous parts [25], as given below:

$$\mathbf{S} = \mathbf{S}^{\mathrm{e}} + \mathbf{S}_{\mathrm{visco}} = (\mathbf{S}_{\mathrm{vol}} + \mathbf{S}_{\mathrm{iso}}) + \mathbf{S}_{\mathrm{visco}}, \tag{5}$$

with:

$$\mathbf{S}_{\mathrm{vol}} = Jp\mathbf{C}^{-1}, \qquad p = \frac{d\psi_{\mathrm{vol}}(J)}{dJ}, \tag{6}$$

$$\mathbf{S}_{\mathrm{iso}} = 2\frac{\partial \psi_{\mathrm{iso}}}{\partial \mathbf{C}} = 2\left(\frac{\partial \psi_{\mathrm{iso}}}{\partial \bar{\mathbf{C}}} : \frac{\partial \bar{\mathbf{C}}}{\partial \mathbf{C}}\right) = 2\left(\frac{\partial \psi_{\mathrm{iso}}}{\partial \bar{I}_1}\frac{\partial \bar{I}_1}{\partial \bar{\mathbf{C}}} + \frac{\partial \psi_{\mathrm{iso}}}{\partial \bar{I}_2}\frac{\partial \bar{I}_2}{\partial \bar{\mathbf{C}}}\right) : \frac{\partial \bar{\mathbf{C}}}{\partial \mathbf{C}}, \tag{7}$$

$$\mathbf{S}_{\mathrm{visco}} = 2\frac{\partial \psi_{\mathrm{visco}}}{\partial \dot{\mathbf{C}}} = 2\left(\frac{\partial \psi_{\mathrm{visco}}}{\partial \dot{\bar{\mathbf{C}}}} \sim \frac{\partial \dot{\bar{\mathbf{C}}}}{\partial \dot{\mathbf{C}}}\right), \tag{8}$$

$\mathbf{S}^{e}$ represents the hyperelastic part, whereas invariants of the modified right Cauchy-Green deformation tensor $\bar{I}_\alpha$ ($\alpha = 1, 2$) are expressed by Eq. (9) [28]:

$$\bar{I}_1 = tr\left(\bar{\mathbf{C}}\right) \qquad \bar{I}_2 = \frac{1}{2}\left[\left(tr\bar{\mathbf{C}}\right)^2 - tr\bar{\mathbf{C}}^2\right]. \tag{9}$$

Here, in order to obtain good fitting with the experimental data, different models are investigated, as shown in the following equations [25,28-30].

The isochoric energy part, ψ_{iso}, is expressed as a function of $(\bar{I}_1 - 3)$ and $(\bar{I}_2 - 3)$ that ensures the strain-zero energy for the zero strain, as shown in Eqs. (10) to (12), which are known as Mooney-Rivlin, Generalized Mooney-Rivlin, and Mansouri models, respectively:

$$\psi_{\mathrm{iso}} = c_{10}\left(\bar{I}_1 - 3\right) + c_{01}\left(\bar{I}_2 - 3\right), \tag{10}$$

$$\psi_{\mathrm{iso}} = c_{10}\left(\bar{I}_1 - 3\right) + c_{01}\left(\bar{I}_2 - 3\right) + c_{11}\left(\bar{I}_1 - 3\right)\left(\bar{I}_2 - 3\right), \tag{11}$$

$$\psi_{\mathrm{iso}} = A\left(e^{m\left(\bar{I}_1 - 3\right)} - 1\right) + B\left(e^{n\left(\bar{I}_2 - 3\right)} - 1\right), \tag{12}$$

where c_{ij}, A, B, m, and n are the material parameters, which must be experimentally determined. The volumetric and short-term viscous energy parts are given as follows:

$$\psi_{\mathrm{vol}} = \frac{k}{2}(J-1)^2, \tag{13}$$

$$\psi_{\mathrm{visco}} = \frac{\eta}{4}\left(\bar{I}_1 - 3\right)\bar{J}_2. \tag{14}$$

$\bar{J}_2$ is the invariant of $\dot{\bar{\mathbf{C}}}$ and defined as follows:

$$\bar{J}_2 = \frac{1}{2}\left(\mathbf{I} : \dot{\bar{\mathbf{C}}}^2\right). \tag{15}$$

2.2. Numerical implementation of model

The advantage of the proposed model in Section 2.1 is that it can be simply used for numerical implementation. For this purpose, the material parameters appearing in the constitutive law need to be identified first with a uniaxial compression test.

2.2.1. Stress-stretch relationship in one dimension

Assuming that a cylindrical sample of isotropic and homogeneous tissues is only compressed in one direction, e.g., z-direction, the deformation gradient tensor, $\mathbf{F}$, can be written as follows:

$$\mathbf{F} = \begin{bmatrix} \lambda^{-\nu} & 0 & 0 \\ 0 & \lambda^{-\nu} & 0 \\ 0 & 0 & \lambda \end{bmatrix}. \tag{16}$$

The modified right Cauchy-Green deformation tensor, $\bar{\mathbf{C}}$, is as follows:

$$\bar{\mathbf{C}} = \begin{bmatrix} \lambda^{\frac{-2-2\nu}{3}} & 0 & 0 \\ 0 & \lambda^{\frac{-2-2\nu}{3}} & 0 \\ 0 & 0 & \lambda^{\frac{4+4\nu}{3}} \end{bmatrix}. \tag{17}$$

Therefore, the invariants are calculated as follows:

$$\bar{I}_1 = 2\lambda^{\frac{-2-2\nu}{3}} + \lambda^{\frac{4+4\nu}{3}},$$

$$\bar{I}_2 = \lambda^{\frac{-4-4\nu}{3}} + 2\lambda^{\frac{2+2\nu}{3}}. \tag{18}$$

Next, the non-zero component of the Cauchy stress tensor during a compression test at time $t = \tau$ has the following form:

$$\sigma_z(t) = F_{\mathbf{z}}(t)\, S_z(t)\, F_z^{\mathrm{T}}(t), \tag{19}$$

where the component of the second Piola-Kirchhoff stress tensor, $S_z(t)$, which defines the stress in compression loading, can be computed through Eq. (5).

In addition, the stress component of the relaxation test corresponding to the loading direction can be calculated through Eqs. (2) and (3), as given below:

$$\sigma_z(t) = \lambda S_z(t)\, \lambda \left[(1 - \alpha(\lambda))\, e^{-t\beta\left(\lambda,\dot{\lambda}\right)} + \alpha(\lambda) \right]. \tag{20}$$

Details of the calculation $S_z(t)$ for the three strain energy functions mentioned in Section 2.1 will be obtained in Appendix.

2.3. Experimental data

To predict the nonlinear behavior of soft tissue via the developed model, material parameters must be determined. The presented model is investigated for Adiprene-L100, a polyurethane-based rubber, as a tissue phantom. Material parameters of the hyperviscoelastic constitutive model are identified with experimental data reported by Khan et al. [31]. Considering that the details of experimental methods for these data are described in [31,32], they will only be briefly discussed. Cylindrical samples from Adiprene-L100 were investigated under the uniaxial compression and stress-relaxation tests. Compression loadings were performed in a wide range of strain rates ($10^{-5} \leq \dot{\varepsilon} \leq 5000\ \mathrm{s}^{-1}$) up to a true strain level of 55%. A stress-relaxation test was also performed under a loading strain rate of $1\ \mathrm{s}^{-1}$. During these tests, the samples were loaded up to 5%. Next, the displacement of a loading plane was held constant for 2 hours, and the behavior of the material was recorded.

3. Results

3.1. Experimental results

The experimental data outlined in [31] present the true stress-true strain and true stress-time curves from uniaxial compression at five different strain rates and a stress-relaxation test, as shown in Figures 1 and 2.

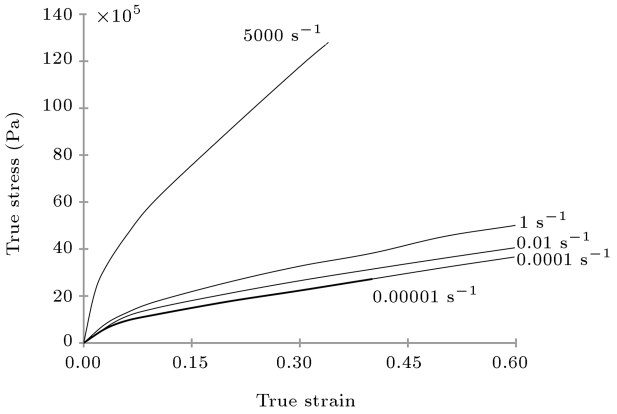

Figure 1. True stress-true strain curves for uniaxial compression test at different levels of strain rates [31].

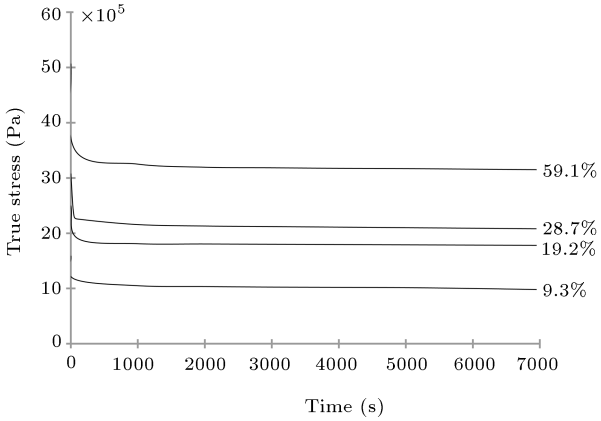

Figure 2. True stress-time curves for stress-relaxation test at different levels of strain at a strain rate of $1\ \mathrm{s}^{-1}$ [31].

Figure 1 shows that stress increases with an increase in strain rates, as has been reported for the other polymers in [18,20]. The linking of smaller units or monomers results in the phenomenon. At a lower loading rate, monomers are reconfigured, and molecular chains can follow the direction of loading. However, at higher rates of loading, because the decentralization and the off-slip between the chains cannot follow the rate of loading at the same speed, the stiffness of the material increases. This data was used to estimate the material parameters that appeared in the proposed constitutive model.

3.2. Estimated material parameters

3.2.1. Hyperelastic material parameters

To describe the nonlinear response of tissue phantom, a strain energy function needs to be chosen for the best fitting with the experimental data. Thus, the hyperelastic material parameters for three strain energy functions, nominated in Section 2.1, are obtained. The parameters are estimated by fitting Eq. (19), assuming $\eta = 0$, with uniaxial compression data by mathematical software at a quasi-static strain rate ($10^{-5}s^{-1}$), as tabulated in Table 1. In Figure 3, the predicted results of different models of the strain energy function and those obtained by experimental data are displayed. Here, true strain is defined as the instantaneous elongation per unit length of the specimen and true stress is calculated using Eq. (19). It is observed that the Generalized Mooney-Rivlin model matches quite well with experimental quasi-static uniaxial compression data. This strain energy function is chosen to describe the true stress-true strain response of tissue-equivalent material under a static condition. As shown in a research study by Khan and Lopez-Pamies [32], $\nu = 0.49$ is obtained for the tested material.

3.2.2. Viscous material parameters

With the hyperelastic parameters determined, the parameter η, considering viscous effect in the constitutive model, can be estimated by fitting Eq. (19) with true stress-true strain curves at strain rates of 10^{-4}, 10^{-2}, 1, and 5000 s^{-1} (Figure 4). The obtained viscous parameters for different strain rates are mentioned in Table 2.

In the next step, by using estimated hyperelastic and viscous parameters, the behavior of tissue phantom (Adiprene-L100) can be predicted in the uniaxial compression test.

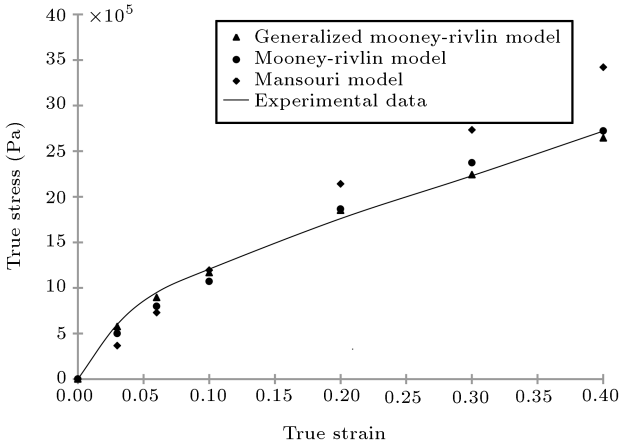

Figure 3. The true stress-true strain curves of uniaxial compression test for tissue phantom at a quasi-static strain rate.

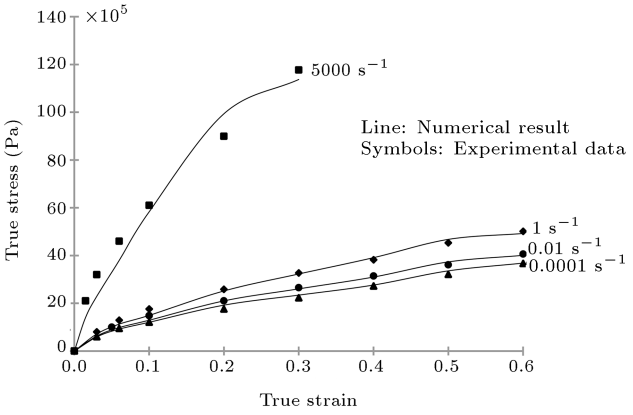

Figure 4. Experimental data and numerical results of uniaxial compression test at strain rates equal to 0.0001, 0.01, 1, and 5000 s^{-1}.

Table 1. Material parameters obtained by the identification of the constitutive models.

Mooney-Rivlin model	$c_{10} = -2.50492e7$ (Pa), $c_{10} = -1.32242e6$ (Pa)	$k = 4.3552e9$
Mansouri model	$A = 1409040$ (Pa), $B = -3366060$ (Pa), $m = -2$, $n = 0.221163$,	$k = 100e6$
Generalized Mooney-Rivlin model	$c_{10} = -7.37708e7$ (Pa), $c_{01} = -2.62259e7$ (Pa), $c_{11} = 1.71906e6$ (Pa)	$k = 1.88022e10$

Table 2. Viscous parameter for different strain rates.

$\dot{\varepsilon}$ (s^{-1})	0.0001	0.01	1	5000
η (Pa.s)	1.78944e9	4.15062e7	853319	11077

3.3. Stress-relaxation response

In this section, experimental data from the stress-relaxation test in constant strain ranging from 9.3% to 59.1% are collected in Figure 2. The whole data are obtained at a strain rate of 1 s^{-1}. Eq. (20) is separately fitted with experimental data in different strain percentages of 19.2%, 28.7%, and 59.1% by the nonlinear least-squares algorithm (Figure 5). Then, values of α and β parameters are determined. Accordingly, by increasing λ, α increases, while β tends to decrease.

Next, a suitable curve is fitted with the obtained values (Figures 6 and 7). Considering the performed investigations, the best functions of α and β are as follows:

$$\alpha(\lambda) = a\lambda^2 + b\lambda + c, \qquad \beta\left(\lambda, \dot{\lambda}\right) = \dot{\lambda}(a\lambda + b).$$

In such a case, the dependence of the tensorial-relaxation function at the strain levels can be obtained.

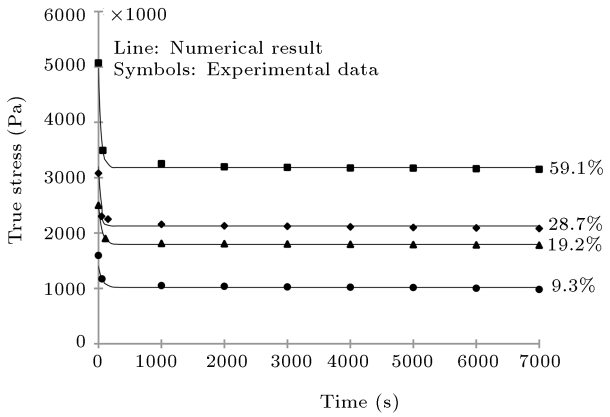

Figure 5. Stress-relaxation curves at strain equal to 9.3%, 19.2%, 28.7%, and 59.1%.

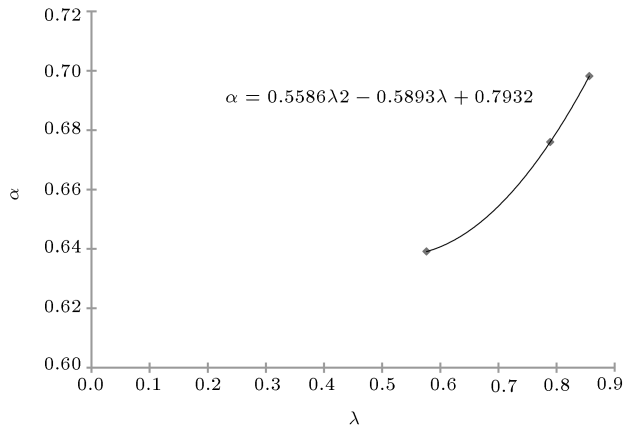

Figure 6. Value of $\alpha(\lambda)$ versus stretch.

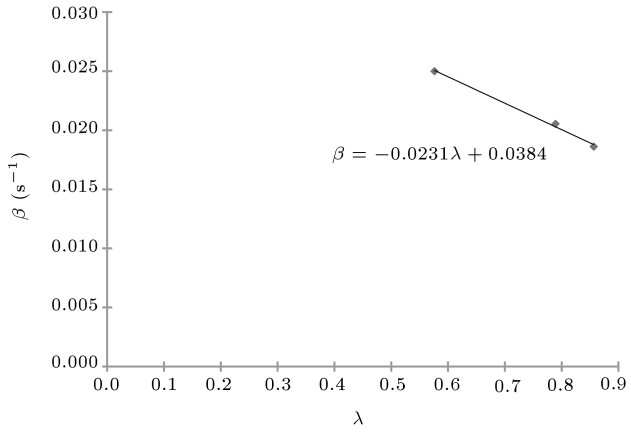

Figure 7. Value of $\beta\left(\lambda, \dot{\lambda}\right)$ at a strain rate of 1 s^{-1} versus stretch.

4. Discussions

In this study, a new nonlinear hyperviscoelastic constitutive model was developed in order to describe the behavior of isotropic and homogeneous soft tissues within the integral framework presented by Pipkin and Rogers. The model was constructed based on the hyperelastic and viscous parts. The hyperelastic part was represented by the strain energy function. The strain energy function was additionally decoupled into isochoric and volumetric sections. Moreover, viscous stress was derived using two short-term and long-term parts. The short-term viscous function characterizes the strain rate sensitivity, while the long-term viscous function considers the deformation history, which is formulated through a nonlinear integrand. The hyperelastic model is not able to account for predicting the relaxation data, and quasi-linear viscoelastic models presented for soft material fail to describe the material behavior during stress-relaxation at different strain levels. However, this limitation was removed in the presented model by introducing an integrand based on the strain level using the functions of $\alpha(\lambda)$ and $\beta\left(\lambda, \dot{\lambda}\right)$.

The constitutive model involves a number of material parameters. The values of those are identified from experimental data for Adiprene-L100 as a tissue-equivalent material. The elastic parameters are estimated by curve-fitting the compression data of the test at a quasi-static strain rate. To achieve this purpose, the Generalized Mooney-Rivlin model was used as the best-fitting on the experimental data associated with the quasi-static strain rate to describe the isochoric stress part of the uniaxial compression response of material. Moreover, with the existence of the parameter in the volumetric part of the strain energy function, the compressibility of the material can be taken into account.

In addition, the stress data of higher strain load-

ing rate are used to determine the viscous parameter, η. These values seem high (Table 2). The very high values for viscous parameters can be found in the literature [28,33]. The model cannot determine a certain viscous parameter at all strain rates because the amplitude of the strain rate range is very wide. Therefore, we fit the constitutive relation on the experimental data of the compression test for each strain rate. In the last step of determining the material parameters, the functions of $\alpha(\lambda)$ and $\beta\left(\lambda,\dot{\lambda}\right)$ are captured by the stress-relaxation data. Figures 4 and 5 show the experimental data and obtained numerical results by the presented model. It is seen that the presented model can follow the experimental data.

In order to verify the constitutive model, values for α and β are estimated by means of substituting the stretch corresponding into strain, $\varepsilon = 9.3\%$, in the represented functions of $\alpha(\lambda)$ and $\beta\left(\lambda,\dot{\lambda}\right)$, which are shown in Figures 6 and 7. Then, the calculated stress at this strain level is plotted in Figure 5 using Eq. (20). Note that the values of the parameters c_{10}, c_{01}, k, and η are fixed to those estimated by fitting Eq. (19) with uniaxial compression data. It is seen that the predicted results agree well with the experimental ones.

The prediction of tissue mechanical behavior by the proposed model can be utilized in the clinical investigations and simulations of tissue/tool interaction in the robotic surgery system. The model can also be used to educate young surgeons by modeling a tissue surgery. Interested readers can extend this model to simulate the heat transfer during laser therapy in patients with advanced cancer.

5. Conclusions

In this study, based on the integral framework and using the short- and long-term viscous functions, a nonlinear hyperviscoelastic constitutive model was developed to characterize the mechanical behavior of isotropic tissue-equivalent materials. Here, Adiprene-L100 was chosen as the tissue-phantom, and the experimental data related to this polymeric material were applied to determine the model parameters.

Even though the results obtained through the numerical implementation of the compression and stress-relaxation tests for different strain rates and strain levels clearly indicated that the model could describe nonlinearity and the strain-dependent stress-relaxation response of tissue phantom, there is good agreement between the predicted results and experimental data. However, the constitutive model is subject to several limitations. First, the material parameters should be estimated by experimental data of different loading tests such as multi-axial and shear loading, since a model must be a practical for all loading cases. Second, considering that many tissues are anisotropic and non-homogeneous, the proposed constitutive model should be extended to describe their behavior.

Nomenclature

P	Lagrange multiplier associated with incompressibility
$\mathbf{C}$	Right Cauchy-Green deformation tensors
$\dot{\bar{\mathbf{C}}}$	Time rate of $\bar{\mathbf{C}}$
$\mathbf{F}$	Deformation gradient tensor
J	Determinant of $\mathbf{F}$
k	Material parameter
$\mathbf{S}$	Second Piola-Kirchhoff stress tensor

Greek Letters

$\dot{\varepsilon}$	Strain rate, s^{-1}
η	Material parameters, Pa s
λ	Stretch along the loading direction
ν	Poisson's ratio

Subscript and superscripts

vol	Volumetric part
iso	Isochoric part
visco	Viscous part

References

1. Trawinski, Z., Wojcik, J., Nowicki, A., Olszewski, R., Balcerzak, A., Frankowska, E., Zegadlo, A., and Rydzynski, P. "Strain examinations of the left ventricle phantom by ultrasound and multislices computed tomography imaging", *Biocyber. Biomed. Eng.*, **35**, pp. 255-263 (2015).
2. Bukala, J., Kwiatkowski, P., and Malachowski, J. "Numerical analysis of stent expansion process in coronary artery stenosis with the use of non-compliant ballon", *Biocyber. Biomed. Eng.*, **36**, pp. 145-156 (2016).
3. Eshghi, S.H., Rajabi, H., Darvizeh, A., Nooraeefar, V., Shafiei, A., Mirzababaie Mostofi, T., and Monsef, M. "A simple method for geometric modeling of biological structures using image processing technique", *Sci. Iran.*, **23**(5), pp. 2194-2202 (2016).
4. Przytulska, M., Gierblinski, I., Kuliusz, J., and Skoczylas, K. "Quantitative examination of liver tissue ultrasound elastograms", *Biocyber. Biomed. Eng.*, **31**(4), pp. 75-85 (2011).
5. Zanetti, M.E., Terzini, M., Mossa, L., Bignardi, C., Costa, P., Audenino, A.L., and Vezzoni, A. "A structural numerical model for the optimization of double pelvic osteotomy in the early treatment of canine hip dysplasia", *Vet. Comp. Orthop. Traumatol.*, **4**, pp. 1-9 (2017).

6. Kemper, A.R., Santago, A.C., Stitzel, J.D., Sparks, J.L., and Duma, S.M. "Effect of strain on the material properties of human liver parenchyma in unconfined compression", *ASME J. Biomech. Eng.*, **135**, pp. 1-8 (2013).
7. Rashid, B., Destrade, M., and Gilchrist, M.D. "Mechanical characterization of brain tissue in simple shear at dynamic strain rates", *J. Mech. Behav. Biomed. Mater.*, **28**, pp. 71-85 (2013).
8. Abbasi, A.A., Ahmadian, M.T., Alizadeh, A., and Tarighi, S. "Application of hyperelastic models in mechanical properties prediction of mouse oocyte and embryo cells at large deformations", *Sci. Iran.*, **25**(2), pp. 700-710 (2018).
9. Quapp, K.M. and Weiss, J.A. "Material characterization of human medial collateral ligament", *ASME J. Biomech. Eng.*, **120**, pp. 757-763 (1998).
10. Wang, X., Schoen, J.A., and Rentschler, M.E. "Aquantitative comparison of soft tissue compressive viscoelastic model accuracy", *J. Mech. Behav. Biomed. Mater.*, **20**, pp. 126-136 (2013).
11. Sharifi Sedeh, R., Ahmadian, M.T., and Janabi-Sharifi, F. "Modeling, simulation, and optimal initiation planning for needle insertion into the liver", *ASME J. Biomech. Eng.*, **132**, pp. 1-11 (2010).
12. Matin Ghahfarokhi, Z., Moghimi Zand, M., and Salmani Tehrani, M. "Analytical solution and simulation of the liver tissue behavior under uniaxial compression test", *Modares Mechanical Engineering*, **16**(9), pp. 47-56 (1395) (in Persion).
13. Matin Ghahfarokhi, Z., Salmani Tehrani, M., Moghimi Zand, M., and Mahzoon, M. "A computational study on the effect of different design parameters on the accuracy of biopsy procedure", *J. A. MECH.*, **46**(2), pp. 221-231 (2015).
14. Troyer, K.L., Shetye, S.S., and Puttlitz, C.M. "Experimental characterization and finite element implementation of soft tissue nonlinear viscoelasticity", *ASME J. Biomech. Eng.*, **134**, pp. 1-8 (2012).
15. Zanetti, E.M., Perrini, M., Bignardi, C., and Audenino, A.L. "Bladder tissue passive response to monotonic and cyclic loading", *Biorheol.*, **49**, pp. 49-63 (2012).
16. Natali, A.N., Audenino, A.L., Artibani, W., Fontanella, C.G., Carniel, E.L., and Zanetti, E.M. "Bladder tissue biomechanical behavior: Experimental tests and constitutive formulation", *J. Biomech.*, **48**, pp. 3088-3096 (2015).
17. Oflaz, H. "A biomechanical comparison between tissue stiffness meter and shore type 00 durometer using fresh human fetal membrane cadavers", *Biocyber. Biomed. Eng.*, **36**, pp. 138-144 (2016).
18. Khajehsaeid, H., Baghani, M., and Naghdabadi, R. "Finite strain numerical analysis of elastomeric bushings under multi-axial loadings: a compressible visco-hyperelastic approach", *Int. J. Mech. Mat. Des.*, **9**, pp. 385-399 (2013).
19. Naghdabadi, R., Baghani, M., and Arghavani, J. "A viscoelastic constitutive model for compressible polymers based on logarithmic strain and its finite element implementation", *Finite Elem. Anal. Des.*, **62**, pp. 18-27 (2012).
20. Karimi, A., Navidbakhsh, M., and Beigzadeh, B. "A visco-hyperelastic constitutive approach for modeling polyvinylalcohol sponge", *Tissue Cell*, **46**, pp. 97-102 (2014).
21. Tirella, A., Mattei, G., and Ahluwalia, A. "Strain rate viscoelastic analysis of soft and highly hydrated biomaterials", *J. Biomed. Mat. Res.*, **102A**(10), pp. 3352-3360 (2014).
22. Miller, K. "Constitutive model of brain tissue suitable for finite element analysis of surgical procedures", *J. Biomech.*, **32**, pp. 531-537 (1999).
23. Pipkin, A.C. and Rogers, T.G. "A nonlinear integral representation for viscoelastic behavior", *J. Mech. Phys. Solids.*, **16**, pp. 59-72 (1968).
24. Rajagopal, K.R. and Wineman, A.S. "Response of anisotropic nonlinearly viscoelastic solids", *Math. Mech. Solids.*, **14**, pp. 490-501 (2009).
25. Holzapfel, G.A., *Nonlinear Solid Mechanics. A Continuum Approach for Engineering*, pp. 205-256, Wiley, UK (2000).
26. Holzapfel, G.A. and Gasser, T.C. "A viscoelastic model for fiber-reinforced composites at finite strains: continuum basis, computational aspects and applications", *Comput. Meth. Appl. Mech. Eng.*, **190**, pp. 4379-4403 (2001).
27. Lu, Y.T., Zhu, H.X., Richmond, S., and Middleton, J. "A visco-hyperelastic model for skeletal muscle tissue under high strain rates", *J. Biomech.*, **43**, pp. 2629-2632 (2010).
28. Limbert, G. and Middleton, J. "A constitutive model of the posterior cruciate ligament", *Med. Eng. Phys.*, **28**, pp. 99-113 (2006).
29. Laksari, k., Sadeghipour, K., and Darvish, K. "Mechanical response of brain tissue under blast loading", *J Mech Behav Biomed Mater*, **32**, pp. 132-144 (2014).
30. Mansouri, M. and Darijani, H. "Constitutive modeling of isotropic hyperelastic materials in an exponential framework using a self- contained approach", *Int. J. Solids Struct.*, **51**(25), pp. 4316-4326 (2014).
31. Khan, A.S., Lopez-Pamies, O., and Kazmi, R. "Thermo-mechanical large deformation response and constitutive modeling of viscoelastic polymers over a wide range of strain rates and temperatures", *Int. J. Plas.*, **22**, pp. 581-601 (2006).
32. Khan, A.S. and Lopez-Pamies, O. "Time and temperature dependent response and relaxation of a soft polymer", *Int. J. Plas.*, **18**, pp. 1359-1372 (2002).
33. Limbert, G. and Middleton, J. "A transversely isotropic viscohyperelastic material application to the modeling of biological soft connective tissues", *Int. J. Solis Struct.*, **41**(15), pp. 4237-4260 (2004).

Appendix

Simplification of formulation $S_z(t)$ for the three strain energy functions

In this section, the stress $S_z(t)$ is formulated by substituting Eqs. (10) to (14) into Eqs. (5) to (8), for three identified strain energy functions in Section 2.

(i) Mooney-Rivlin model:

$$\begin{aligned}S_z(t) = \lambda^{2\nu}\Bigg[&k\left(\lambda^{(1-4\nu)} - \lambda^{(-2\nu)}\right)\\ &+ \frac{4}{3}c_{10}\left(\lambda^{\frac{-2+4\nu}{3}} - \lambda^{\frac{-2-8\nu}{3}}\right)\\ &+ \frac{4}{3}c_{01}\left(\lambda^{\frac{-4+2\nu}{3}} - \lambda^{\frac{-10-4\nu}{3}}\right)\\ &+ \lambda^{\frac{-2+4\nu}{3}}\Bigg\{\dot{\lambda}(\bar{I}_1-3)\Bigg[\frac{\eta(4+4\nu)}{6}\lambda^{\frac{1+4\nu}{3}}\\ &-\frac{\eta}{6}\lambda^{-2}\Bigg(\frac{-4-4\nu}{3}\lambda^{\frac{-5-8\nu}{3}}\\ &+ \frac{4+4\nu}{3}\lambda^{\frac{7+4\nu}{3}}\Bigg)\Bigg]\Bigg\}\Bigg].\end{aligned} \tag{A.1}$$

(ii) Generalized Mooney-Rivlin model:

$$\begin{aligned}S_z(t) = \lambda^{2\nu}\Bigg[&k\left(\lambda^{(1-4\nu)} - \lambda^{(-2\nu)}\right)\\ &+ \frac{4}{3}c_{10}\left(\lambda^{\frac{-2+4\nu}{3}} - \lambda^{\frac{-2-8\nu}{3}}\right)\\ &+ \frac{4}{3}c_{01}\left(\lambda^{\frac{-4+2\nu}{3}} - \lambda^{\frac{-10-4\nu}{3}}\right)\\ &+ 4c_{11}\Bigg(\lambda^{(2\nu)} - \lambda^{\frac{-2+4\nu}{3}} - \lambda^{\frac{-4+2\nu}{3}}\\ &- \lambda^{(-4-2\nu)} + \lambda^{\frac{-8-2\nu}{3}} + \lambda^{\frac{-10-4\nu}{3}}\Bigg)\\ &+ \lambda^{\frac{-2+4\nu}{3}}\Bigg\{\dot{\lambda}(\bar{I}_1-3)\Bigg[\frac{\eta(4+4\nu)}{6}\lambda^{\frac{1+4\nu}{3}}\\ &- \frac{\eta}{6}\lambda^{-2}\Bigg(\frac{-4-4\nu}{3}\lambda^{\frac{-5-8\nu}{3}}\\ &+ \frac{4+4\nu}{3}\lambda^{\frac{7+4\nu}{3}}\Bigg)\Bigg]\Bigg\}\Bigg].\end{aligned} \tag{A.2}$$

(iii) Mansouri model:

$$\begin{aligned}S_z(t) = \lambda^{2\nu}\Bigg[&k\left(\lambda^{(1-4\nu)} - \lambda^{(-2\nu)}\right)\\ &+ \frac{4}{3}\lambda^{\frac{1+4\nu}{3}}\left(1 - \lambda^{(-2-2\nu)}\right)\\ &+ \left(Ame^{m(\bar{I}_1-3)} + Bn\bar{I}_1e^{n(\bar{I}_2-3)}\right)\\ &+ \left(Bne^{n(\bar{I}_2-3)}\right)\left(-\lambda^{\frac{4+4\nu}{3}} + \lambda^{\frac{-8-8\nu}{3}}\right)\\ &+ \lambda^{\frac{-2+4\nu}{3}}\Bigg\{\dot{\lambda}(\bar{I}_1-3)\Bigg[\frac{\eta(4+4\nu)}{6}\lambda^{\frac{1+4\nu}{3}}\\ &- \frac{\eta}{6}\lambda^{-2}\Bigg(\frac{-4-4\nu}{3}\lambda^{\frac{-5-8\nu}{3}}\\ &+ \frac{4+4\nu}{3}\lambda^{\frac{7+4\nu}{3}}\Bigg)\Bigg]\Bigg\}\Bigg].\end{aligned} \tag{A.3}$$

Biographies

Zahra Matin Ghahfarokhi received her BS degree in Mechanical Engineering of Biosystem from Shahrekord University, Iran in 2008 and her MS degree in Mechanical Engineering from the same institute in 2011. Now, she is researching as a PhD student in Mechanical Engineering at the Department of Mechanical Engineering, Isfahan University of Technology, Isfahan, Iran.

Mahdi Moghimi Zand is a Faculty Member in the School of Mechanical Engineering, College of Engineering, University of Tehran and Director of Small Medical Devices, Bio-MEMS and LoC Lab. His research is multi-disciplinary and revolves around vibrations, MEMS, computational mechanics, bio-medical engineering, and nano technology. He also has had different research and visiting faculty positions at Georgia Technology, Sharif University of Tech, Michigan State University and University of Tehran.

Mehdi Salmani-Tehrani completed his undergraduate studies, MSc, and PhD degrees, all at the Isfahan University of Technology, Iran. He is now an Assistant Professor at the Isfahan University of Technology, where he has been a faculty member since 2011. His research interest mainly focuses on metal forming analysis and, recently, on biomechanics studies.